Two-layer model of anisotropy beneath Myanmar and Thailand revealed by shear-wave splitting

Kasemsak Saetang[*,1]

[1] Program in Physics, Faculty of Education, Nakhon Si Thammarat Rajabhat University, Nakhon Si Thammarat, 80280, Thailand

Abstract

The first model of two layers is presented to study the anisotropy pattern beneath Myanmar and Thailand using shear-wave splitting. Teleseismic activity recorded by 15 permanent broadband stations was analysed to investigate the anisotropy and to understand the flow direction in the mantle. The flow direction and speed were observed in the forms of fast polarisation direction (ϕ) and delay time (δt) between fast and slow components. The measurements showed that a two-layer model beneath stations better explicates the splitting observations than a single-layer model. The upper and lower layers were interpreted as lithosphere and asthenosphere in similar patterns and compared with GPS (Global Positioning System) velocity fields and strain rate fields. Two groups of ϕ can be classified and matched with West-Burma Terrane (WBT) and Shan-Thai Terrane (STT). The ϕ represents that West-Burma Terrane moves in a northward direction, Shan-Thai Terrane and Indo-China Terrane (ICT) move in a south-eastern direction, and West-Burma Terrane has less anisotropy of ϕ than Shan-Thai Terrane.

Keywords: Anisotropy; Myanmar; Shear-wave splitting; SplitRacer, Thailand

1. Introduction

Shear-wave splitting (SWS) measurements have been widely used to observe anisotropy in the earth from the crust down to the core-mantle boundary [Wüstefeld et al., 2008]. The SWS occurs when the wave travels through anisotropic media [Gök et al., 2003] and splits into two waves that travel with different velocities and different polarization. The splitting is parameterised by the ϕ (fast polarisation direction) and the δt, which is the different travel-time between fast and slow waves. These two terms provide descriptions of an anisotropic medium. In the upper mantle, seismic anisotropy results from the lattice-preferred orientation (LPO) of mantle minerals [Long, 2009]. The SWS measurements are an essential indicator to obtain upper-mantle anisotropy. The fast direction of anisotropy beneath measured stations can be used to identify the local flow geometry of the mantle.

The study area is located in Myanmar and Thailand (Figure 1). The area is the junction of three terranes; West-Burma Terrane, Shan-Thai Terrane, and Indo-China Terrane [Charusiri et al., 1993; Morley et al., 2011]. West-Burma Terrane is the extension of the West Sumatra block; it was separated by the formation of the Andaman Sea in the Miocene [Barber and Crow, 2009]. GPS velocity fields published by Kreemer et al. [2014], Maurin et al. [2010],
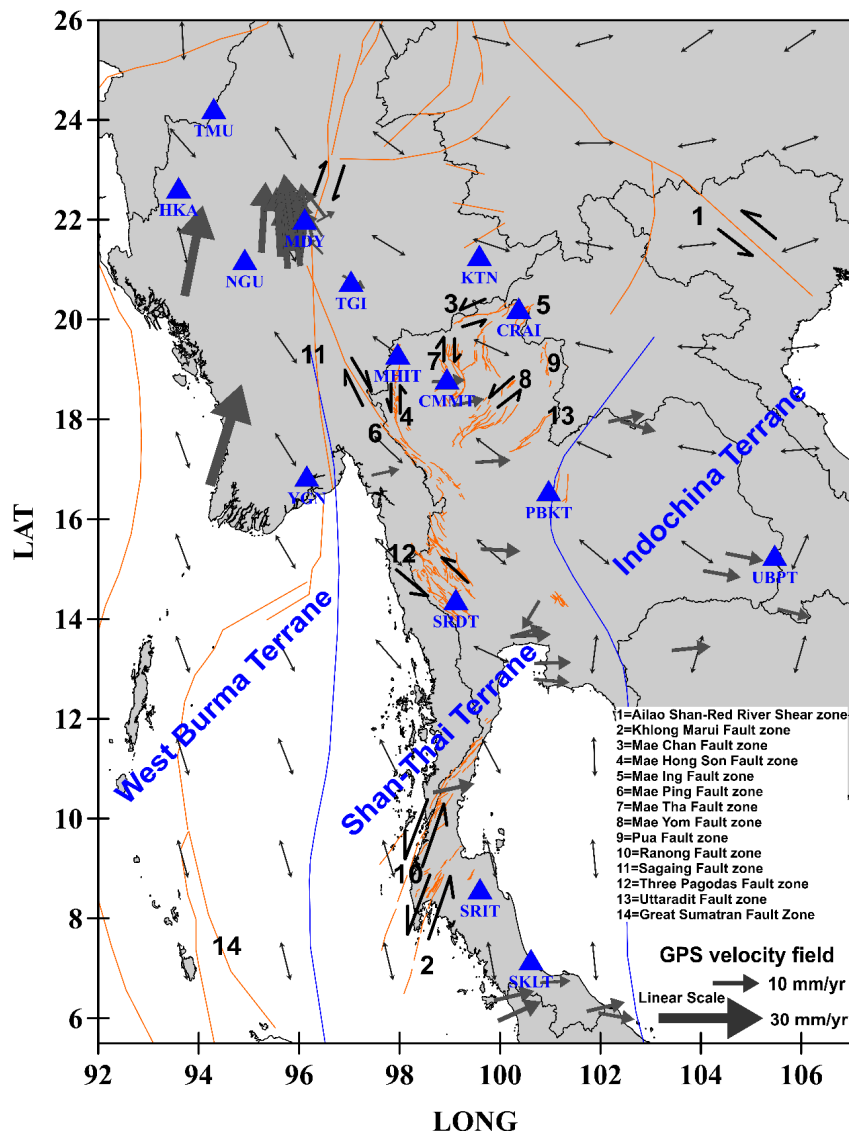
Figure 1. GPS velocity and strain rate fields, seismic stations, and tectonic setting [Charusiri et al., 1993; DMR, 2007; Morley et al., 2011]. Single- and double- black arrows are plate movements [Kreemer et al., 2014; Maurin et al., 2010; Simons et al., 2007; UNAVCO] and extensional directions [Hao et al., 2019] measured by GPS stations. Seismic stations for SWS measurements are plotted as blue triangles. Blue and orange lines denote terrane boundaries and faults.

Simons et al. [2007] show that the West-Burma Terrane moves in a northward direction. Shan-Thai Terrane moves in an eastward direction, which can be traced through Thailand into southern China and includes the western part of the Malay peninsula and eastern Sumatra. Indo-China Terrane, which moves in a south-eastern direction, forms the core of Southeast Asia, separated from Gondwana in the Late Devonian. GPS velocity fields (arrow length) also indicate that the West-Burma Terrane moves faster than the Shan-Thai Terrane and the Indo-China Terrane. The strain rate field from Hao et al. [2019] plotted in Figure 1 indicated that the extensional directions of the West-Burma Terrane, Shan-Thai Terrane, and Indo-China Terrane, lie approximately as the NW-SE direction, NW-SE and N-S directions, and NW-SE and E-W directions, respectively.

Several fault systems appear in the left and right lateral strike-slip faults. Three Pagodas fault zone and Mae Ping fault zone have north-western–south-eastern (NW-SE) directions with left-lateral and right-lateral strike slips [Searle and Morley, 2011]. The Sagaing fault zone in Burma shows a right-lateral strike-slip and connects to the Mae Ping fault zone. The southern part of Thailand comprises the Khlong Marui fault zone and Ranong fault zone, and both are left lateral strike slips. Complex fault systems are in the northern part of Thailand. There are left and right lateral strike slips with north-south (N-S) and north-eastern–south-western (NE-SW) directions. Although

the Ailao Shan-Red River shear zone early moved in left lateral strike-slip, GPS measurements found active right-lateral movements.

Although the SWS measurement was studied in this area, it was done using a one-layer model [Kong et al., 2018; Wongwai et al., 2020; Yu et al., 2018] in Thailand and the Ailao Shan-Red River shear zone (Figure 7d). This research used three-component seismic stations to estimate the splitting parameters beneath stations. The results, geological information, and GPS velocity fields were used to interpret the shear wave splitting throughout the study area. The anisotropy patterns were discussed for a two-layer model.

2. Data and Method

Data and methods were run and controlled by the software SplitRacer [Reiss and Rümpker, 2017]. This code was designed to measure teleseismic shear-wave splitting by minimising transverse energy [Silver and Chan, 1991]. The 15 seismic stations used in this study are operated by MM (Myanmar National Seismic Network) and TM (Thai Seismic Monitoring Network) networks (see Figure 1). MM and TM are the network codes used by the International Federation of Digital Seismograph Networks (FDSN) and the Incorporated Research Institutions for Seismology (IRIS). Seismic data of the earthquakes with a magnitude above six were downloaded using the IRIS Web Services; the considered time interval is from the stations' deployment time (Table 1) until October 31, 2018. The three kinds of shear waves selected are SKS, SKKS, and PKS phases (all called XKS phases). These phases provide the best lateral resolution due to the steep angle of the incidence. The epicentral distances are in a range of 85°-180° [Reiss and Rümpker, 2017] to cover the XKS phases. The arrival times of theoretical phases at the stations were calculated using an Earth model IASP 91. The SWS measurements require the definition of an analysis window which was manually selected, starting from the calculated XKS arrival times. The signals were bandpass filtered between 4 and 50 s. A signal-to-noise (SNR) ratio above 2 was chosen to collect XKS phases from events. The difference between the

Station name	Lat.	Long.	Stations' deployment time (IRIS, n.d.-a, n.d.-b)	Upper layer		Lower layer		No. of measurements	
				ϕ (°)	δt (s)	ϕ (°)	δt (s)	good/fair	null
CMMT	18.81	98.94	2009-01-01	−70	0.8	50	0.6	42	8
CRAI	20.22	100.37	2008-01-01	20	1.0	−60	1.4	19	2
HKA	22.64	93.60	2016-01-20	0	2.4	30	0.4	56	1
KTN	21.28	99.59	2016-01-26	−80	1	−70	0.2	26	3
MDY	22.01	96.11	2016-01-14	−10	0.4	−30	0.6	36	1
MHIT	19.31	97.96	2008-01-01	20	2.4	−60	1.6	30	6
NGU	21.20	94.91	2017-08-10	0	1.2	30	1.8	13	1
PBKT	16.57	100.96	2008-01-01	60	1.0	−80	0.4	20	1
SKLT	7.17	100.61	2008-01-01	−60	1.4	50	0.2	19	4
SRDT	14.39	99.12	2008-01-01	−80	1.6	20	1.4	28	5
SRIT	8.59	99.60	2008-01-01	−20	0.2	10	2.2	20	3
TGI	20.76	97.03	2017-08-10	50	0.4	−30	0.8	16	3
TMU	24.23	94.30	2016-01-17	10	0.8	20	0.4	27	13
UBPT	15.27	105.47	2008-01-01	−30	1.4	50	1.2	13	7
YGN	16.86	96.15	2016-01-11	40	0.4	−40	1.6	23	2

Table 1. SWS measurements of 15 seismic stations.

event's back azimuth and the major axis of the ellipse of long-period particle motions was used to see the sensor misalignments [Rümpker and Silver, 1998] as shown in Figure 2. The sensor misalignments were calculated from all XKS measurements at a station, and the values outside one standard deviation from the mean were skipped.
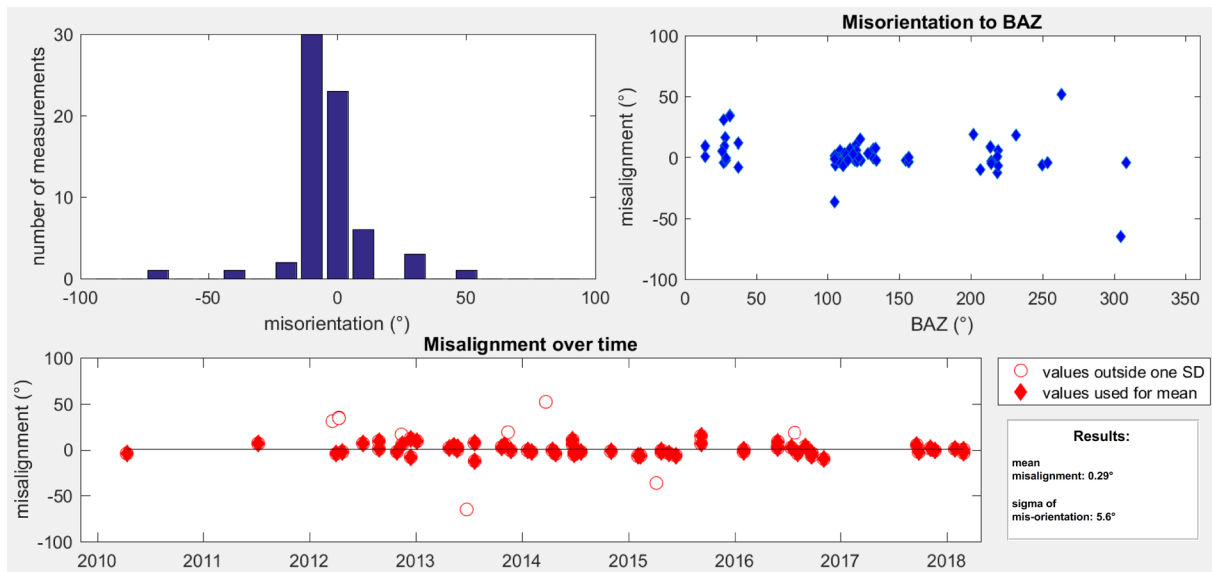

Figure 2. A check of station misalignments of data for station CMMT. The top left is a histogram plot that indicates the variation of misalignment values. The top right is the dot plot between misalignment values and back azimuth. The bottom is the misalignment of values over time. The filled and open red circles are used and unused data due to being inside and outside one standard deviation of the mean value.

A standard single-phase SWS measurement is based on the energy minimisation method [Silver and Chan, 1991]. This method is the most stable one when noise is detected and utilizes a grid

search approach to identify the pair of ϕ and δt which best minimizes the amount of energy on the transverse component when the effect of splitting is accounted for [Long and Silver, 2009]. A grid search method [Silver and Chan, 1991] is used to find the splitting parameters (ϕ and δt). The resolutions were automatically set into 1° for values (0°-180°) of ϕ, and 0.1s for values (0-4 s) of δt (Figure 3) to find the best parameters. Due to the statistical analysis, 50 slightly shifted time windows were created by starting with the original time defined by manual pre-processing steps, and the time windows were automatically set around the original time. These are critical results for analysis with a single time-window because many cases showed that different windows give very different results [Reiss and Rümpker, 2017; Teanby et al., 2004]. The histograms in Figure 3c show the results of the splitting parameters for 50 slightly shifted time windows at station CMMT. Although the SNR is high, the author decided to reject the SWS measurements that do not show the same direction for varying results in the statistical analysis. Only stable measurements over different windows were accepted.

The SWS measurements were categorised into good, fair, poor, and null, following Reiss and Rümpker [2017]. A good measurement has the apparent phase of the XKS arrivals on both radial and transverse components, near elliptical particle motion, no or only minor scattering in histogram plots of the splitting parameters, a small 95% confidence level, and a linearisation of the particle motion after removing the energy from the transverse component. Fair measurement has the same characteristic as good measurement but with more noise included while still being above 50% of energy reduction. A poor measurement has nonelliptical particle motion, energy removal of less than 50%, and high scattering of the results of the splitting parameters. Finally, null measurement occurs when there is no anisotropy along the ray path, or when the initial polarization is parallel or perpendicular to the fast axis of the anisotropic medium [Reiss and Rümpker, 2017]. The SWS analysis often shows an unusually high delay time, and an energy grid indicates minimum energy on two different fast polarisation directions and a large confidence level [Reiss and Rümpker, 2017]. The good and fair SWS measurements from the single-phase analysis were used to discover the exact solution of the splitting parameters.
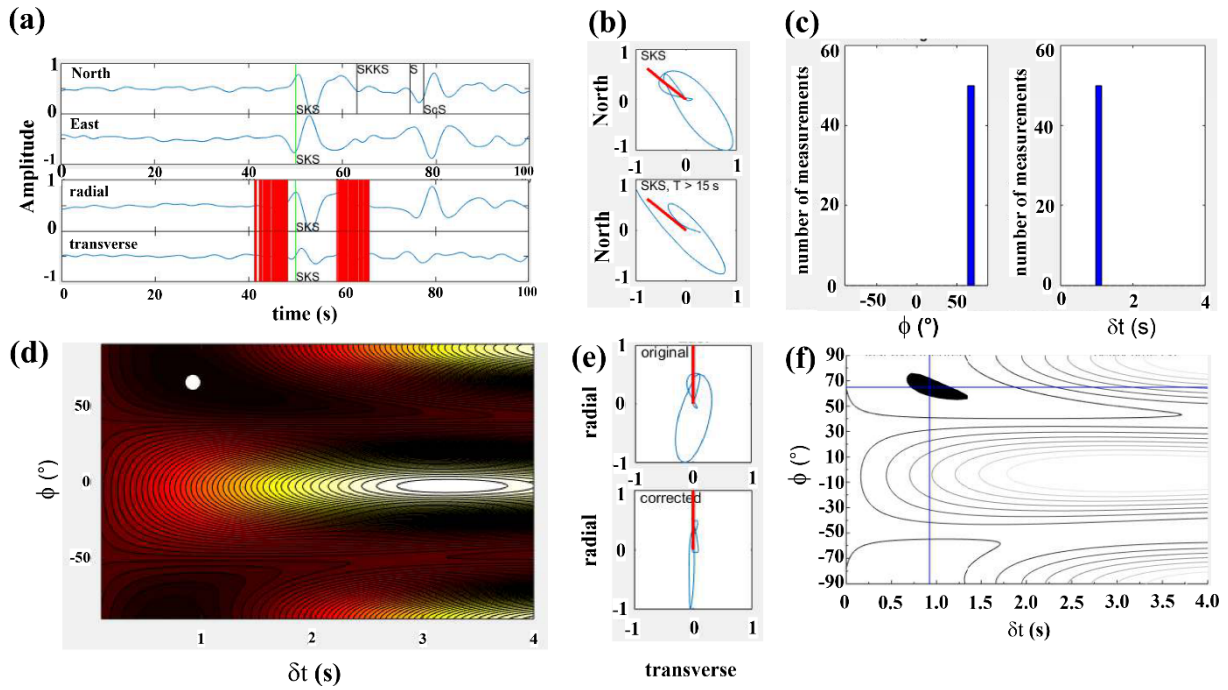
Figure 3. An example of a single-phase splitting analysis at station CMMT, origin time: April 11, 2010, at 22:08:12, BAZ: 308.5°, distance: 88.4°. a) North/East and radial/transverse components. The green line indicates the theoretical phase arrival. The red lines show the 50 different time windows used for the analysis. b) The top and bottom figures are particle motions of the XKS (here SKS) window for the unfiltered trace and 15 s low-pass filtering. The theoretical back azimuth is shown in the red line. c) The histograms of all splitting measurements show the distribution over the 50-time windows. d) Energy grid. The white dot marks the splitting parameters with an average energy grid. e) Original and corrected particle motions. f) The 95% confidence level is referred to by the black contour. The blue cross indicates the best energy minimisation on the transverse component of the splitting parameters.
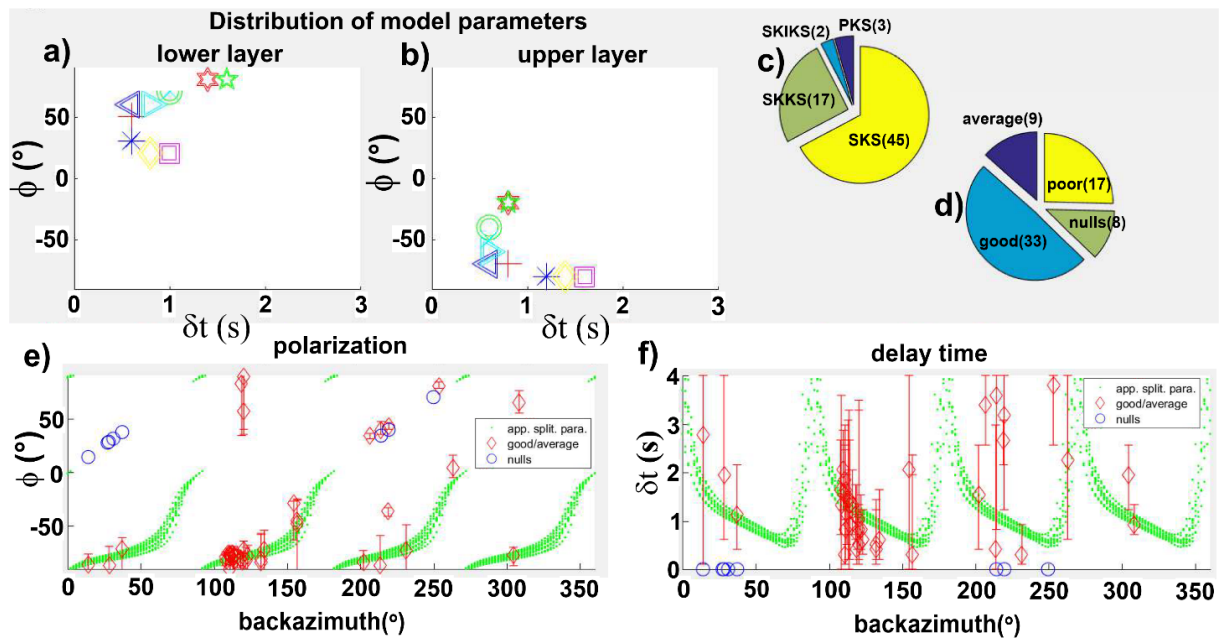

Figure 4. Single splitting analysis using a two-layer model for station CMMT. a) and. b) The ten best-fitting models of lower and upper layers. c) The distribution of used phases. d) The quality classification of events. e) and. f) show the ϕ and the δt as functions of back azimuth, respectively, from the ten best-fitting models. The values obtained for the ϕ and the δt are $-70°$, 0.8 s of an upper layer and 50°, 0.6 s of a lower layer.

The splitting parameters were separately plotted as a function of the back azimuth to consider one- or two-layer models (Figure 4e and Figure 4f). The number of events is essential to identify one- or two-layer models with a proper back azimuth coverage. The results of stations that cannot identify one- or two-layer models due to insufficient back-azimuth coverage were not presented in Table 1. One-layer model is found if the splitting measurements do not show significant dependence as function of back azimuth, and a mean value is calculated (Reiss & Rümpker, 2017). Conversely, the splitting parameters identify a two-layer model if a function of back azimuth with $\frac{\pi}{2}$ periodicity is observed (Savage, 1999).

All possible models using steps of 10° of ϕ and 0.2 s of δt were investigated for fitting the two-layer model with apparent (measured) splitting parameters [Reiss and Rümpker, 2017; Silver & Savage, 1994]. The ten best-fitting models are automatically calculated using apparent splitting parameters in the SplitRacer software to find the best fitting, reported in Table 1, and illustrated in Figure 5 and Figure 6.

3. Results and Discussion

The results of the splitting parameters beneath 15 stations and null measurements are presented. The length of the error bars in Figure 5 shows that the model of ϕ is more stable than δt. Because of this uncertainty in the δt model, we plotted the magnitude scale for δt in Figure 7 and presented the value for δt in Table 1 without any discussion, while only ϕ models will be discussed. The function of back azimuth with $\frac{\pi}{2}$ periodicity in Figure 5 indicates that a two-layer model better explains the observations than a single-layer model for all stations. The distribution of the ten best-fitting models shows the characteristics of the models (Figure 6). The stations CMMT, CRAI, MHIT, PBKT, SKLT, SRDT, SRIT, TGI, UBPT, and YGN show that the group of ten best-fitting models separate into negative and positive values of ϕ either for the upper or for the lower layer. The group of the ten best-fitting models in Figure 6 from upper-layer model of KTN, upper- and lower- layer models of HKA, upper-layer model of MDY, upper-layer model of SKLT, upper- and lower- layer models of TMU, lower-layer model of SRIT, and lower-layer model of YGN show approximately horizontal lines that indicate larger stability of ϕ models than δt models. On the contrary, the results of upper-layer SRIT and upper-layer YGN show vertical lines that indicate the δt models are more stable than ϕ models.

Lattice-preferred orientation (LPO) of mantle minerals, such as olivine and flow-induced strain generally results in the shear-wave splitting of seismic waves that travel through the mantle. Bai et al. [2009] summarised the research and reported that SWS splitting is most sensitive to the upper mantle. This paper also assumes that the source of SWS splitting comes from the upper mantle and interpreted the two-layer model as associated with lithosphere and asthenosphere. The splitting parameters identify the two-layer model as a function of back azimuth with $\frac{\pi}{2}$ periodicity [Savage, 1999)]. The number of events is essential to identify one-layer or two-layer models with appropriate back azimuth coverage. In this paper, only 15 stations were selected with enough back-azimuth coverage to discriminate between one-layer or two-layer models.

We not only considered geological information, but also GPS velocity and strain rate fields (Figure 1) and findings from previous studies (Figure 7d). The SWS results beneath Thailand from Wongwai et al. [2020] demonstrated a one-layer model. The stations that show the N-S and E-W directions for ϕ are located within Shan-Thai Terrane and Indo-China Terrane, respectively. The SWS study of Southeast Asia by Yu et al. [2018] showed that the E-W direction of ϕ is observed in the northern Indochina Peninsula while mostly N-S direction of ϕ is observed on SE Tibetan Plateau. Kong et al. [2018] inspected a two-layered anisotropy structure beneath the transitional region between the S-E Tibetan Plateau and the Indochina Peninsula. The upper-layer model of ϕ was compared to the crust and the lower-layer model was interpreted as the flow of the upper asthenosphere in the E-W direction.

Here that the upper layer in Figure 7a is interpreted as the lithosphere. If ϕ is related to GPS velocity fields, the kinematic models between the lithosphere and shallow deformation are considered as not different [Chang et al., 2006]. If ϕ and plate motion are not parallel, the anisotropy comes from the relationship between plate motions and mantle flows [Gök et al., 2003]. From results in Figure 7a related to GPS velocity field, the author interprets the flow direction of the lithosphere using blue arrows. The ϕ values are grouped into northward directions and south-eastern directions for West-Burma Terrane and Shan-Thai Terrane. Direction patterns of ϕ clearly change at the boundaries of West-Burma Terrane and Shan-Thai Terrane.
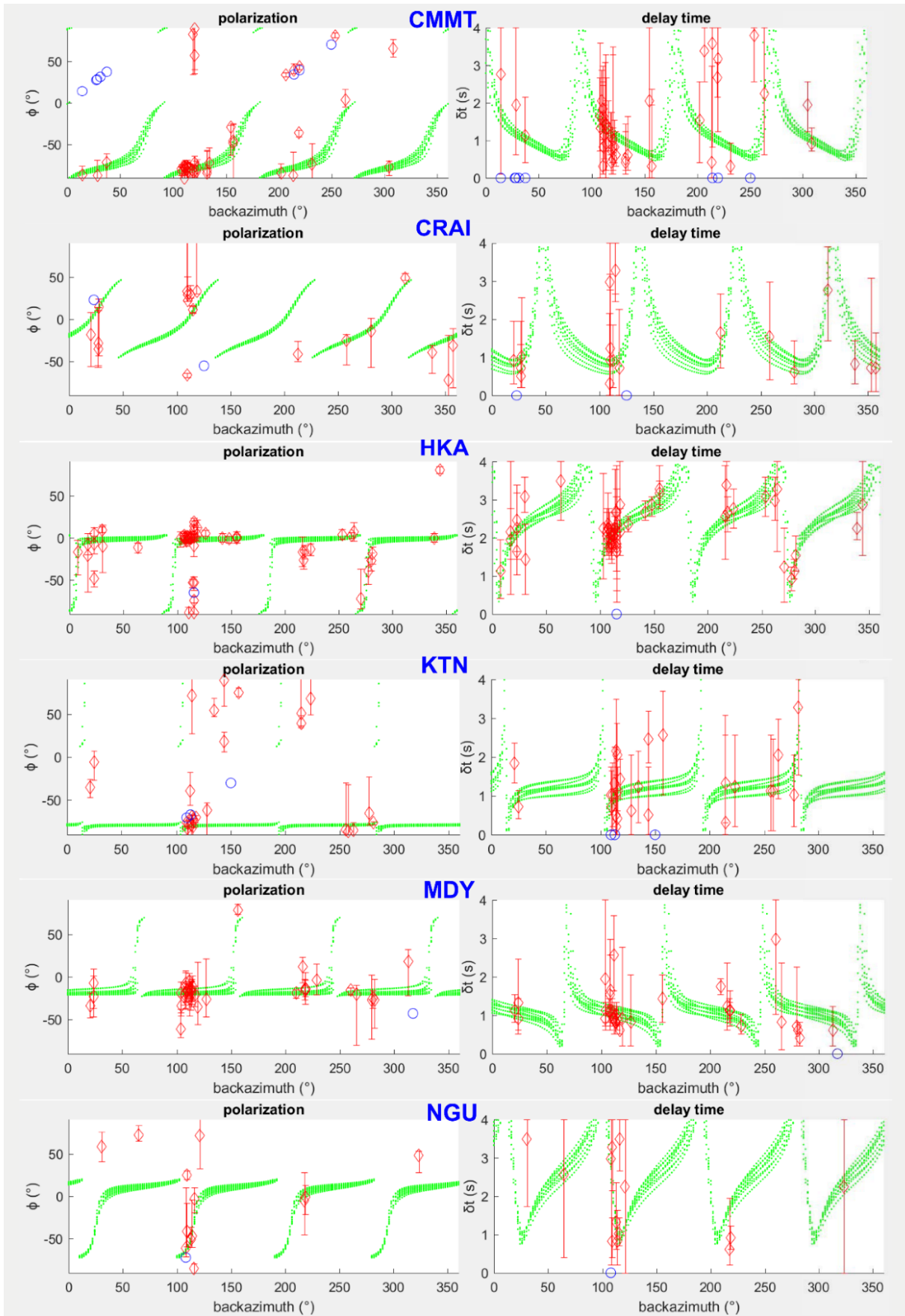
Figure 5. The ϕ and the δt in single splitting using a two-layer model were plotted as functions of back azimuth. The apparent splitting parameters resulting from the ten best-fitting models are denoted as green dots. Good/fair measurements are shown by red diamonds with error bars; null measurements as blue circles.
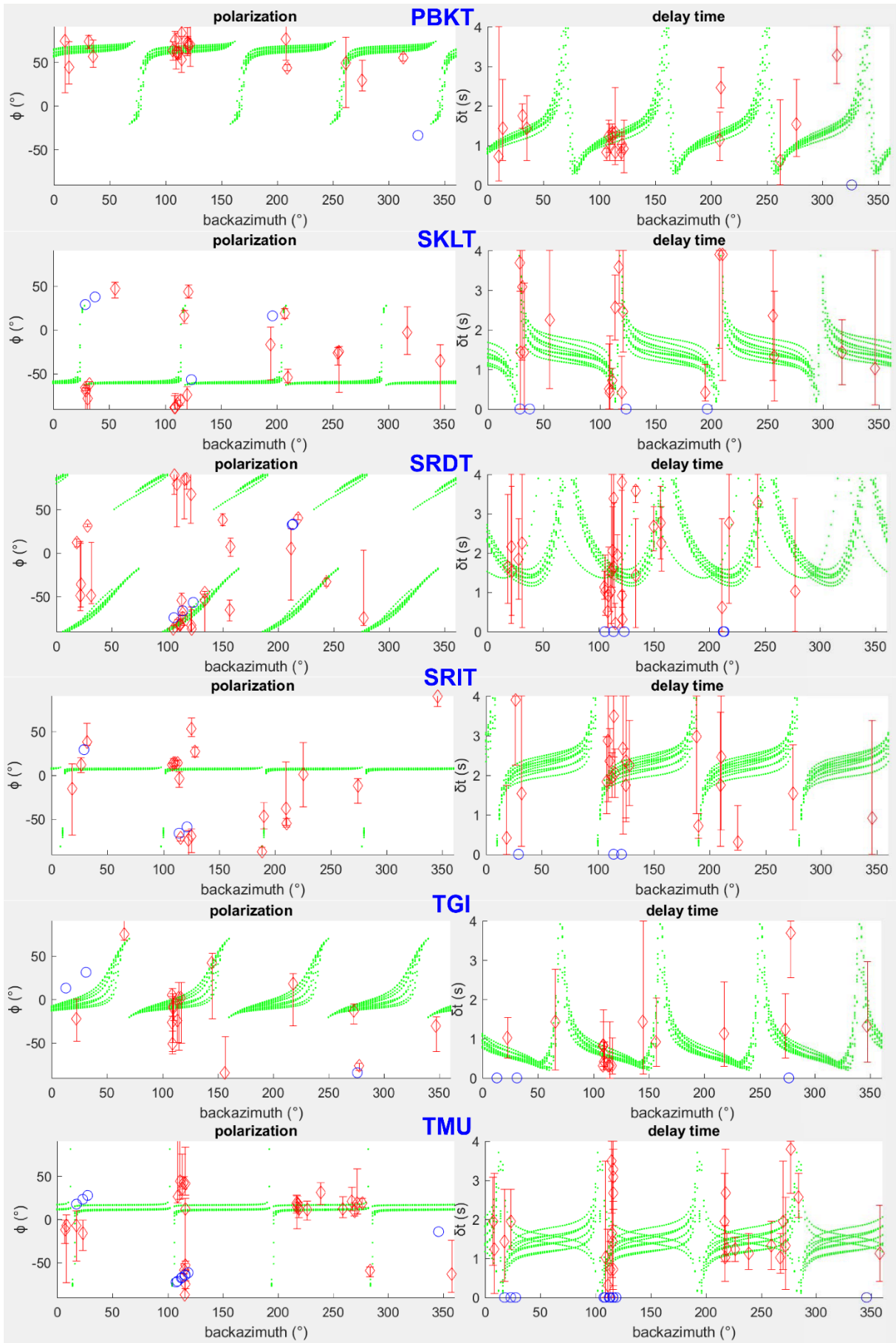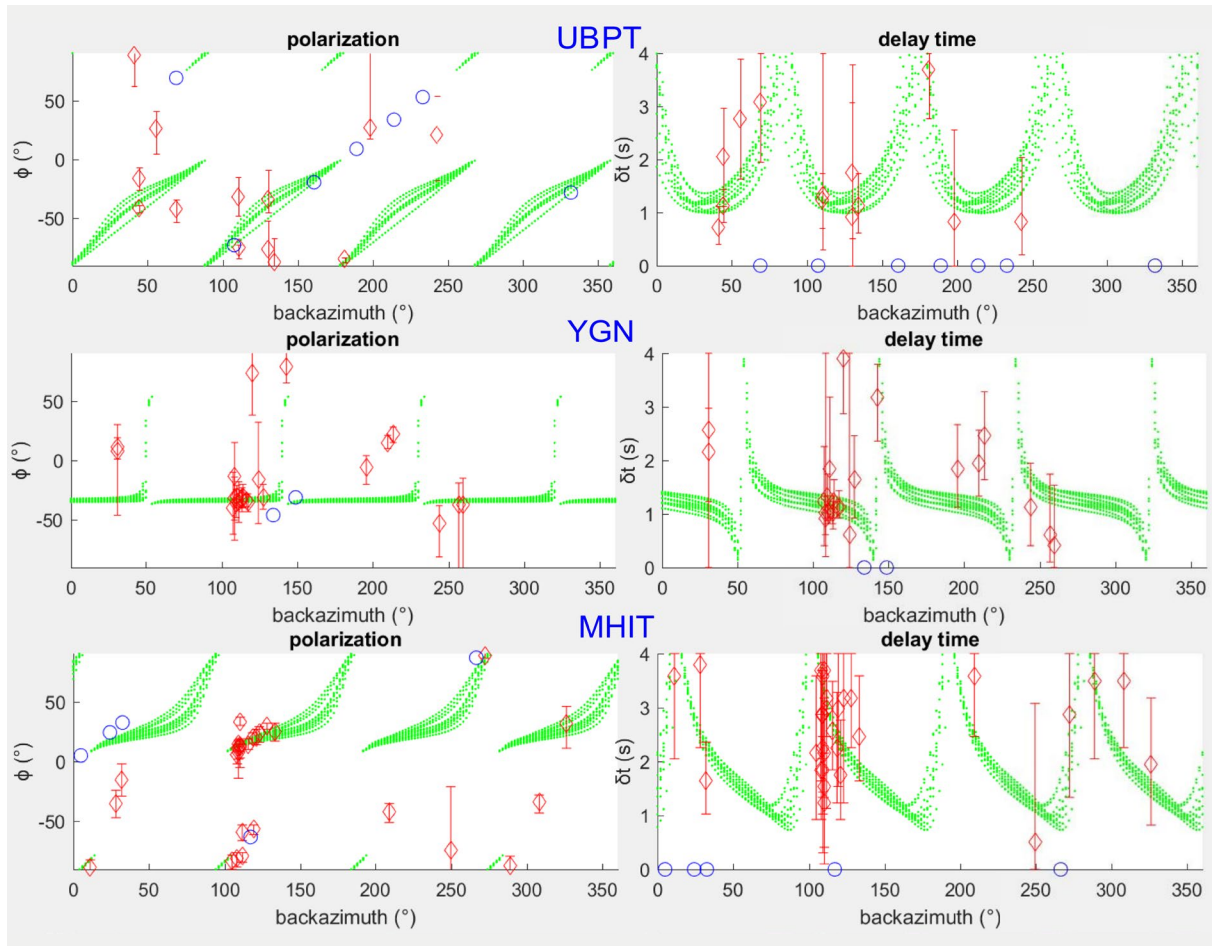
Figure 5. (continuous)

Figure 5. (continuous)

The ϕ value of the upper layer beneath most stations is related to GPS velocity fields. The ϕ of four stations (HKA, MDY, NGU, TMU) located in West-Burma Terrane is generally N-S trending with the flow direction of lithosphere interpreted in a northward direction. The ϕ value of Shan-Thai Terrane shows results in many directions at several stations. These are interpreted from the interactions of several plates [Huang et al., 2015]. The ϕ values of CRAI and MHIT are parallel to near-fault strikes (Mae Ing and Mae Hong Son fault zones, respectively). The ϕ values of CMMT, KTN, and SRDT are compared with GPS velocity fields and are interpreted to result from the south-eastern-flow direction of the lithosphere. ϕ of SKLT and SRIT located in Southern Thailand do not correlate with near-fault strikes of the Khlong Marui fault zone (KMFZ) and the Ranong fault zone (RFZ). The station PBKT is located at the boundary between Shan-Thai Terrane and Indo-China Terrane; the lithosphere-flow direction is interpreted along the north-eastern direction. The station UBPT located in Indo-China Terrane is jointly considered with GPS velocity fields and interpreted in the SSE direction. These findings indicate that the flow of the lithosphere for Shan-Thai Terrane is not related to the fault systems.

The lower layer in Figure 7b is interpreted as the asthenosphere beneath Thailand and Myanmar, estimated to be at an 80 km depth [Tianfeng, 2016]. The ϕ values are compared with the upper-layer model and GPS velocity fields. Jolivet et al. [2018] interpreted the crust and the asthenosphere flow directions beneath East Asia and showed similar patterns. Here, the author assumes that the flow directions beneath Myanmar and Thailand linked with East Asia have the same patterns. The general view also indicates that ϕ beneath most stations is related to GPS velocity fields. The ϕ values of the five stations located in West-Burma Terrane were interpreted with the help of GPS velocity and strain rate fields and show the flow direction of the asthenosphere in the north-eastern direction for HKA, NGU, and TMU, and in the north-western direction for MDY, and YGN. The ϕ value of the five stations located in Shan-Thai Terrane (CRAI, KTN, MHIT, PBKT, and TGI) is also consistent with GPS velocity and strain rate fields in the south-eastern direction. P wave tomography from Huang et al. [2015] demonstrated a south-eastern-flow direction of the lithosphere and asthenosphere beneath Shan-Thai terrane, where the station KTN
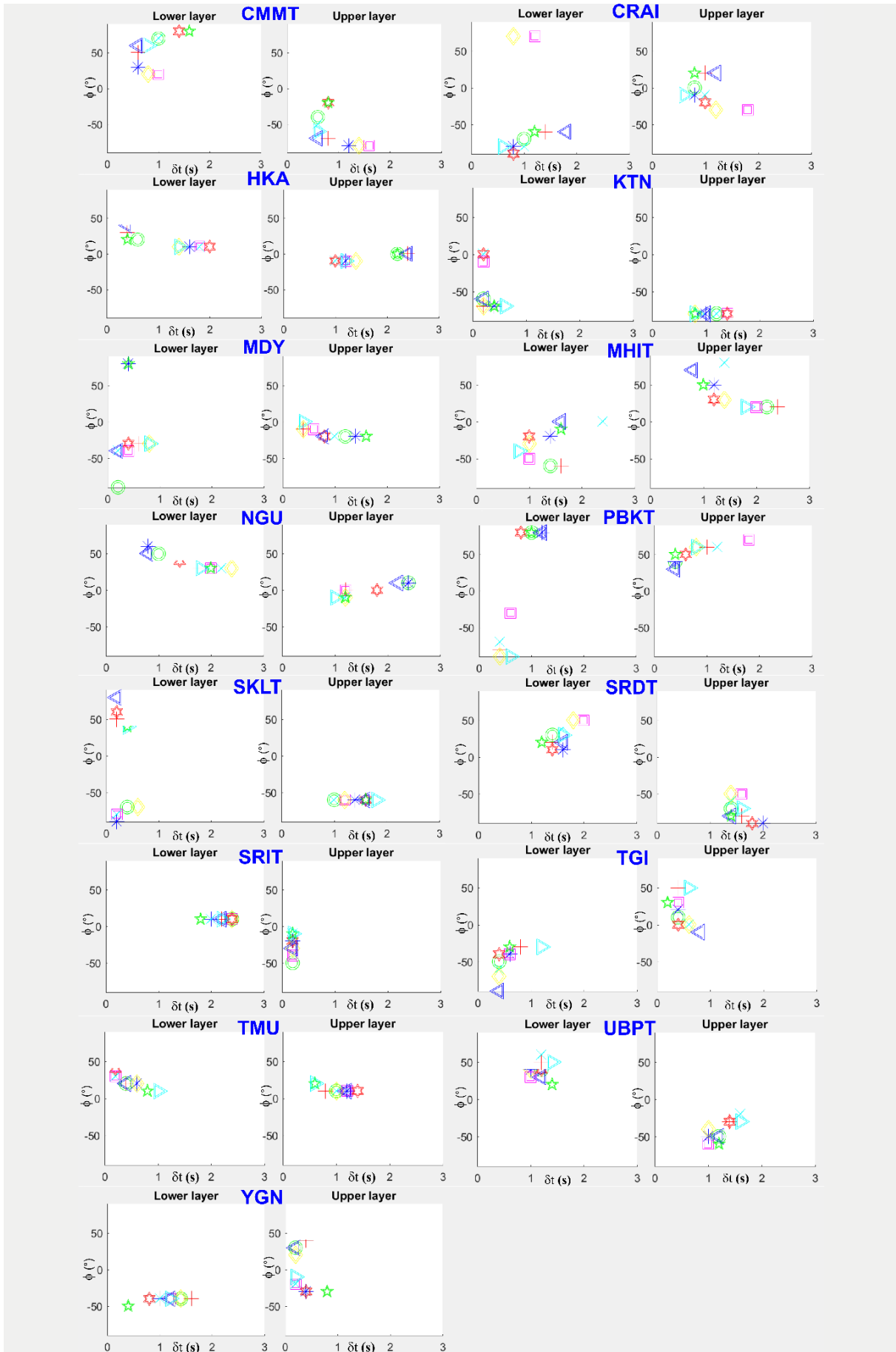
Figure 6. Distribution of the ten best-fitting models for upper and lower layers.
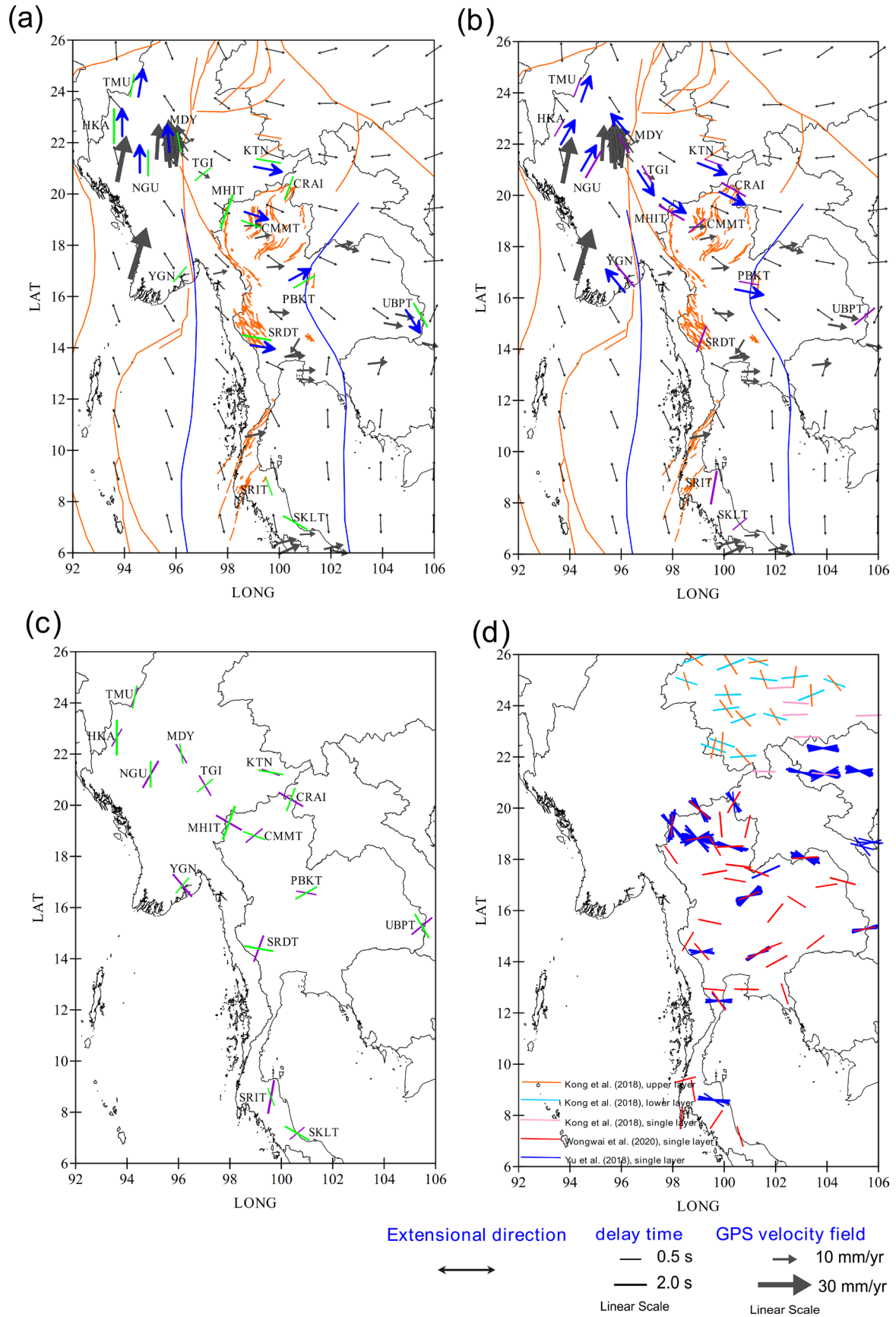
Figure 7. Results of Table 1 in the two-layer model of the anisotropy are presented. a) Upper layers (green bars). b) Lower layers (purple bars). The interpretation of flow directions in both layers is drawn by blue arrows. c) The splitting parameters for the upper and lower layers. d) Results of other studies in nearby regions from Kong et al. [2018]; Wongwai et al. [2020]; Yu et al. [2018].

is located. The two seismic stations (CMMT and SRIT) have ϕ values not directly related to GPS velocity fields but parallel to the near-fault strikes of the Mae Tha fault zone and Khlong Marui fault zone, respectively. Figure 7c presents the SWS measurements of the upper and lower layers in the same map when plotted in different colours. KTN and TMU show that the ϕ directions of the upper and lower layers do not significantly differ and are related to the values in Table 1.

4. Conclusions

The measurements of SWS were conducted to describe the pattern of anisotropy beneath Myanmar and Thailand using a two-layer model. All stations indicate that the splitting observations are better explained by a two-layer model than by a single-layer model. The upper and lower layers were interpreted as lithosphere and asthenosphere, with the flow directions beneath most stations related to GPS velocity fields. The ϕ values of West-Burma Terrane, both in the lithosphere and asthenosphere, are the only north-western direction that shows a weaker anisotropy of West-Burma Terrane as compared to the Shan-Thai Terrane. A complex direction of the ϕ value in the Shan-Thai Terrane was observed in both the lithosphere and asthenosphere. Also, the direction flow of the lithosphere and asthenosphere shows a significant difference between West-Burma Terrane and Shan-Thai Terrane.

References

Bai, L., Iidaka, T., Kawakatsu, H., Morita, Y. and N.Q. Dzung (2009). Upper mantle anisotropy beneath Indochina block and adjacent regions from shear-wave splitting analysis of Vietnam broadband seismograph array data, Phys. Earth Planet. Int., 176, 1, 33-43, doi:https://doi.org/10.1016/j.pepi.2009.03.008

Barber, A. J. and M. J. Crow (2009). Structure of Sumatra and its implications for the tectonic assembly of Southeast Asia and the destruction of Paleotethys, Island Arc, 18, 1, 3-20, doi:https://doi.org/10.1111/j.1440-1738.2008.00631.x

Chang, L. J., C. Y. Wang, and Z. F. Ding (2006). A Study on SKS Splitting Beneath the Yunnan Region, Southwestern China, Chinese, J. Geophys., 49, 1, 167-175, doi:10.1002/cjg2.824

Charusiri, P., A. H. Clark, E. Farrar, D. Archibald and B. Charusiri (1993). Granite belts in Thailand: evidence from the 40Ar/39Ar geochronological and geological syntheses, J. Southeast Asian Earth Sci., 8, 1, 127-136, doi:https://doi.org/10.1016/0743-9547(93)90014-G

DMR. (2007). Geological Map of Thailand, Ministry of Natural Resources and Environment, Thailand.

Gök, R., J. F. Ni, M. West, E. Sandvol, D. Wilson, R. Aster, W.S. Baldridge, S. Grand, W. Gao, F. Tillmann and S. Semken (2003). Shear wave splitting and mantle flow beneath LA RISTRA, Geophys. Res: Lett., 30, 12, doi:10.1029/2002gl016616

Hao, M., Y. Li and W. Zhuang (2019). Crustal movement and strain distribution in East Asia revealed by GPS observations, Scientific Reports, 9, 1, 16797, doi:10.1038/s41598-019-53306-y

Huang, Z., D. Zhao and L. Wang (2015). P wave tomography and anisotropy beneath Southeast Asia: insight into mantle dynamics, J. Geophys. Res.: Solid Earth, 120, 7, 5154-5174, doi:10.1002/2015jb012098

IRIS. (n.d.-a). MetaData Aggregator: Network Summary: MM (2016-01-01 - 2599-12-31), Retrieved from https://ds.iris.edu/mda/MM/?starttime=2016-01-20T00:00:00&endtime=2599-12-31T23:59:59

IRIS. (n.d.-b). MetaData Aggregator: Network Summary: TM (2008-01-01 - 2599-12-31), Retrieved from https://ds.iris.edu/mda/TM/?starttime=2009-01-01T00:00:00&endtime=2599-12-31T23:59:59

Jolivet, L., C. Faccenna, T. Becker, M. Tesauro, P. Sternai and P. Bouilhol (2018). Mantle Flow and Deforming Continents: from India-Asia Convergence to Pacific Subduction, Tectonics, 37, 9, 2887-2914, doi:https://doi.org/10.1029/2018TC005036

Kong, F., J. Wu, L. Liu, K. H. Liu, J. Song, J. Li and S. S. Gao (2018). Azimuthal anisotropy and mantle flow underneath the southeastern Tibetan Plateau and northern Indochina Peninsula revealed by shear wave splitting analyses, Tectonophysics, 747-748, 68-78, doi:https://doi.org/10.1016/j.tecto.2018.09.013

Kreemer, C., G. Blewitt and E. C. Klein (2014). A geodetic plate motion and Global Strain Rate Model, Geochem. Geophys., Geosyst., 15(10), 3849-3889, doi:10.1002/2014gc005407

Long, M. D. (2009). Going with the mantle flow, Nature Geosci., 2, 1, 10-11, doi:10.1038/ngeo398

Long, M. D. and P. G. Silver (2009). Shear wave splitting and mantle anisotropy: Measurements, interpretations, and new directions, Surv. Geophys., 30, 4-5, 407-461, https://doi.org/10.1007/s10712-009-9075-1

Maurin, T., F. Masson, C. Rangin, U. T. Min and P. Collard (2010). First global positioning system results in northern Myanmar: constant and localized slip rate along the Sagaing fault, Geology, 38, 7, 591-594, doi:10.1130/G30872.1

Morley, C. K., P. Charusiri and I. M. Watkinson (2011). Structural geology of Thailand during the Cenozoic, In M. F. Ridd, A. J. Barber, & M. J. Crow (Eds.), The Geology of Thailand: Geological Society of London.

Reiss, M. C. and G. Rümpker (2017). SplitRacer: MATLAB Code and GUI for Semiautomated Analysis and Interpretation of Teleseismic Shear-Wave Splitting, Seism. Res. Lett., 88, 2A, 392-409, doi:10.1785/0220160191

Rümpker, G. and P. G. Silver (1998). Apparent shear-wave splitting parameters in the presence of vertically varying anisotropy, Geophys. J. Int., 135, 3, 790-800, doi:10.1046/j.1365-246X.1998.00660.x

Savage, M. K. (1999). Seismic anisotropy and mantle deformation: what have we learned from shear wave splitting?, 37(1), 65-106, doi:10.1029/98rg02075

Searle, M. P. and C. K. Morley (2011). Tectonic and thermal evolution of Thailand in the regional context of SE Asia, In M. F. Ridd, A. J. Barber, & M. J. Crow (Eds.), The Geology of Thailand: Geological Society of London.

Silver, P. G. and W. W. Chan (1991). Shear wave splitting and subcontinental mantle deformation, J. Geophys. Res.: Solid Earth, 96, B10, 16429-16454, doi:10.1029/91jb00899

Silver, P. G. and M. K. Savage (1994). The Interpretation of Shear-Wave Splitting Parameters in the Presence of Two Anisotropic Layers, Geophys. J. Int., 119, 3, 949-963, doi:10.1111/j.1365-246X.1994.tb04027.x

Simons, W. J. F., A. Socquet, C. Vigny, B. A. C. Ambrosius, S. Haji Abu, C. Promthong, C. Subarya, D. A. Sarsito, S. Matheussen, P. Morgan and W. Spakman (2007). A decade of GPS in Southeast Asia: resolving Sundaland motion and boundaries, J. Geophys. Res.: Solid Earth, 112, B6, doi:https://doi.org/10.1029/2005JB003868

Teanby, N. A., J. M. Kendall and M. van der Baan (2004). Automation of Shear-Wave Splitting Measurements using Cluster Analysis, Bull. Seism. Soc. Am., 94, 2, 453-463, doi:10.1785/0120030123

Tianfeng, W. (2016). Discussion on the special lithosphere type in eastern china, Earth Sci., 5, 1, 1, doi:10.11648/j.earth.20160501.11

UNAVCO. GPS Velocity Viewer, Retrieved from https://www.unavco.org/software/visualization/GPS-Velocity-Viewer/GPS-Velocity-Viewer.html

Wongwai, W., P. Pananont, E. Sandvol and K. Furlong (2020). Seismic anisotropy of the upper mantle beneath Thailand: tectonic setting constrained by shear-wave splitting analysis, Songklanakarin J. Sci. Technol., 42, 5, 1098-1105.

Wüstefeld, A., G. Bokelmann, C. Zaroli and G. Barruol (2008). SplitLab: a shear-wave splitting environment in Matlab, Compu. Geosci., 34, 5, 515-528, doi:https://doi.org/10.1016/j.cageo.2007.08.002

Yu, Y., S. S. Gao, K. H. Liu, T. Yang, M. Xue, K. P. Le and J. Gao (2018). Characteristics of the Mantle Flow System Beneath the Indochina Peninsula Revealed by Teleseismic Shear Wave Splitting Analysis, Geochem. Geophys., Geosys., 19, 5, 1519-1532, doi:https://doi.org/10.1029/2018GC007474

*CORRESPONDING AUTHOR: Kasemsak SAETANG,

Program in Physics, Faculty of Education, Nakhon Si Thammarat Rajabhat University, Nakhon Si Thammarat, 80280, Thailand

e-mail: light2529@gmail.com